Strain-driven reversible switching of Radial vortex in a bicomponent nanomagnet*

XIA Yongshun, CUI Huanqing, YANG Xiaokuo, GUO Baojun, DOU Shuqing, KANG Yan, WEI Bo, LIANG Bujia

Fundamentals Department, Air Force Engineering University, Xi'an 710051, China

Abstract

Radial magnetic vortices, characterized by their topological stability and nanoscale dimensions, are considered to be highly promising information carriers in magnetic electronic devices. However, traditional methods of reversing the polarity of radial magnetic vortices, which rely on magnetic fields or spin-polarized currents, encounter significant energy consumption problems. To address this challenge, this study proposes a novel field-free control scheme based on multiferroic heterostructures, consisting of a bicomponent nanomagnet (Terfenol-D/Ni), a heavy metal layer, and a piezoelectric layer. The intrinsic symmetry-breaking property of this structure effectively disrupts the circular symmetry of the radial magnetic vortex, which can make voltage-driven polarity reversal through magnetoelectric coupling effects. $MuMax_3$-based multifield coupling simulations of electro-mechanical-magnetic interactions show that when the ratio of the bicomponent materials $d_{\mathrm{TD}}: d_{\mathrm{Ni}} = 1:2$ and the interfacial Dzyaloshinskii-Moriya interaction (DMI) coefficient (D) is in a range of $1.2\mathrm{mJ/m^2} < D < 1.9\mathrm{mJ/m^2}$, the system stably presents a radial magnetic vortex state. Within this DMI coefficient range, when the thickness of the bicomponent nanomagnet is less than 4 nm, an appropriate radius can be found to ensure that the ground state of the bicomponent nanomagnet is a radial magnetic vortex state. Particularly, when the thickness t = 1 nm, the radius of the bicomponent nanomagnet can remain in the radial magnetic vortex state in a range of 50 ± 10 nm. In addition, this study also verifies that square and elliptical bicomponent nanomagnets each have a ground state of radial magnetic vortex. When $D = 1.7\mathrm{mJ/,m^2}$, only a 90 mV voltage pulse is required to achieve polarity reversal of the bicomponent nanomagnet, with a total energy consumption per bit E_{total} of 5.6 aJ, which is six orders of magnitude lower than that from the traditional methods (reaching the aJ level). Through the simulation of transient magnetization dynamics and the analysis of energy evolution, this study

---

* The paper is an English translated version of the original Chinese paper published in Acta Physica Sinica. Please cite the paper as: XIA Yongshun, CUI Huanqing, YANG Xiaokuo, GUO Baojun, DOU Shuqing, KANG Yan, WEI Bo, LIANG Bujia，**Strain-driven reversible switching of Radial vortex in a bicomponent nanomagnet**. *Acta Phys. Sin.*, 2025,74(16): 168503. doi:10.7498/aps.74.20250575

reveals the physical mechanism of polarity reversal of radial magnetic vortices in this bicomponent multiferroic heterostructure: The energy competition in the bimaterial system driven by strain leads to the reconfiguration of magnetic moments, achieving the polarity reversal with efficient and ultra-low energy consumption. This scheme offers a new path for on-chip integration of magnetic vortex memory, paving the way for a novel paradigm in designing non-current-driven "electric write" magnetic storage devices, which hold significant application value in the field of low-power spintronics.

Keywords:radial magnetic vortex; strain-driven; nanomagnet; magnetoelectric coupling
PACS: 85.75.–d; 75.78.Cd; 75.70.Cn; 75.70.Kw
doi:10.7498/aps.74.20250575
cstr:32037.14.aps.74.20250575

1. Introduction

Magnetic vortex, as a nanoscale magnetic structure, has been widely concerned and favored since its inception because of its small size, easy integration, strong adjustability, low driving current density and low thermal loss, and is regarded as one of the most promising information carriers for magnetoelectronic devices[1,2]. In 2016, Siracusano and others[3] magnetic radial vortex introduced the DMI effect into the magnetic vortex. This interfacial chiral spin-orbit interaction competes with the exchange energy, magnetostatic energy and anisotropy energy in the system to produce a new topological spin structure, the magnetic radial vortex (MRV) structure[3-5]; the Fig. 1 gives the distribution state of the magnetization vector of MRV, which usually contains the in-plane magnetization vector pointing to the boundary or center and perpendicular to the surface. This MRV can be characterized by chirality and polarity. The chirality is defined as R= + 1 when the in-plane magnetization vector points to the boundary and R= – 1 when it points to the center. The polarity is defined as P= + 1 when the central magnetization vector points upward perpendicular to the disk surface and P= – 1 when it points downward perpendicular to the disk surface[6]. The chirality of the MRV's central region is fixed by its polarity, a characteristic arising from the topological constraints imposed by asymmetric IDMI. Therefore, MRV is only a diploid degenerate state, and the radial chirality of MRV can be changed simultaneously by polarity reversal[7]. In 2018, Karakas et al.[8]discovered several topological textures such as MRV and Skyrmion in Pt/CoFeB/Ti multilayer materials, verified the existence of MRV through experiments, and proposed that MRV can be used in ultra-low power devices, such as magnetic vortex oscillators, magnetic vortex memories, and magnetic logic circuits[8-12].

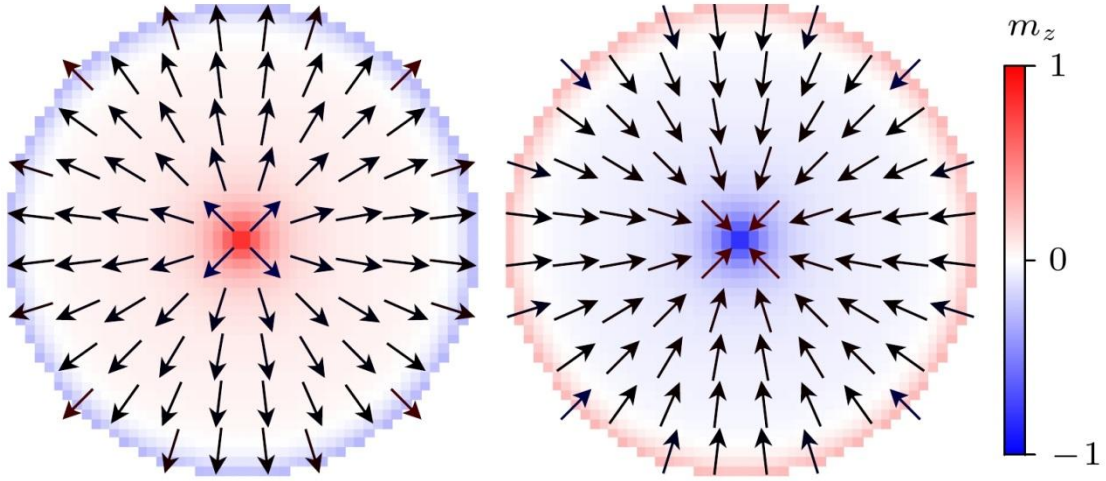

Figure 1. Diagram of magnetic radial vortex

At present, the reversal of MRV polarity mostly depends on the vertical magnetic field pulse or spin-polarized current, but the stimulation of the magnetic field is generated by the current passing through the coil or stripline, which hinders the miniaturization of the device and interferes with the adjacent elements when the target element is excited[13]. In addition to the magnetic field, the MRV polarity can be effectively switched by the threshold current of the $10^6 \mathrm{A/cm}^2$, but the current-driven MRV polarity switching process involves a large vortex core gyration motion, which requires a large enough spin-polarized current, resulting in a considerable charge flow and a significant power consumption problem, which restricts the further development and application of magnetic memory[14,15]. Therefore, it is of great significance to find an ultra-low power MRV polarity reversal method for the practical application of the device. Magnetoelectric coupling effect opens up a potential control path for multiferroic heterostructures, which can achieve efficient and energy-saving control of magnetization state through voltage-induced strain. Recent frontier studies have shown that this strain control can not only achieve magnetization switching, but also effectively manipulate the dynamic behavior of magnetic domain walls and precisely modulate the output characteristics of spin torque oscillators[16]. In 2021, Zhu Mingmin et al. Used strain-driven radial magnetic vortex polarity reversal in geometrically confined multiferroic heterojunctions[17], but this method has strict requirements on the perpendicular anisotropy of the nanomagnet itself. Subsequently, the group designed a strain-controlled spin torque nano-oscillator based on radial magnetic vortices, which can complete binary frequency shift keying and amplitude keying modulation under the cooperation of current pulse and strain pulse[18]. Recently, Valencia et al.[19] used the stray magnetic field of superconductors to imprint radial magnetic vortex structures in circular and square ferromagnets in ferromagnet/superconductor hybrid structures, and achieved high temperature stability, providing a new way to regulate the magnetic structure. In this paper, a bicomponent nanomagnet (Terfenol-D and Ni)/heavy metal layer/piezoelectric layer heterostructure is proposed, which breaks through the limitation of a

single material magnetic layer and innovatively uses two materials with opposite magnetostrictive coefficients to form a bicomponent nanomagnet, and uses the different responses of the two materials to the same strain to achieve field-free strain-controlled MRV polarity reversal.

2. Device structure and theoretical model

The detailed structure of the device is shown in Fig. 2. Above the device is a cylindrical bicomponent nanomagnet disk composed of Ni and Terfenol-D, with a diameter of $d = 100\mathrm{nm}$ and a thickness of $t = 1\mathrm{nm}$. The bicomponent nanomagnet can be experimentally prepared by an oblique deposition-selective etching-lift-off process[20]. The ratio of the two materials in a bicomponent nanomagnet (i.e., ferromagnetic layer, FM) can be controlled, and the lengths of the two materials in the *y* direction are represented by d_{TD} and d_{Ni}, respectively. Beneath the FM is a 5 nm thick heavy metal (HM) layer. In this structure, the DMI effect generated by the FM/HM interface can promote the MRV of the composite magnetic layer nanodisk. Below the HM is a 400 nm thick piezoelectric layer (PMN-PT). When a voltage *U* is applied to the piezoelectric layer in the vertical direction, the strain generated will be transferred to the bicomponent nanomagnet disk above, and then the magnetization state of the bicomponent nanomagnet can be controlled by inverse magnetoelectric coupling. The material parameters of Ni used in this model are[21]: saturation magnetization $M_{\mathrm{S}} = 4.84 \times 10^5 \mathrm{A/m}$, exchange coefficient $A_{\mathrm{ex}} = 1.05 \times 10^{-11} \mathrm{J/m}$, damping coefficient $\alpha = 0.045$; the material parameters of Terfenol-D are[22]: saturation magnetization $M_{\mathrm{S}} = 8 \times 10^5 \mathrm{A/m}$, exchange coefficient $A_{\mathrm{ex}} = 9 \times 10^{-12} \mathrm{J/m}$, damping coefficient $\alpha = 0.1$.

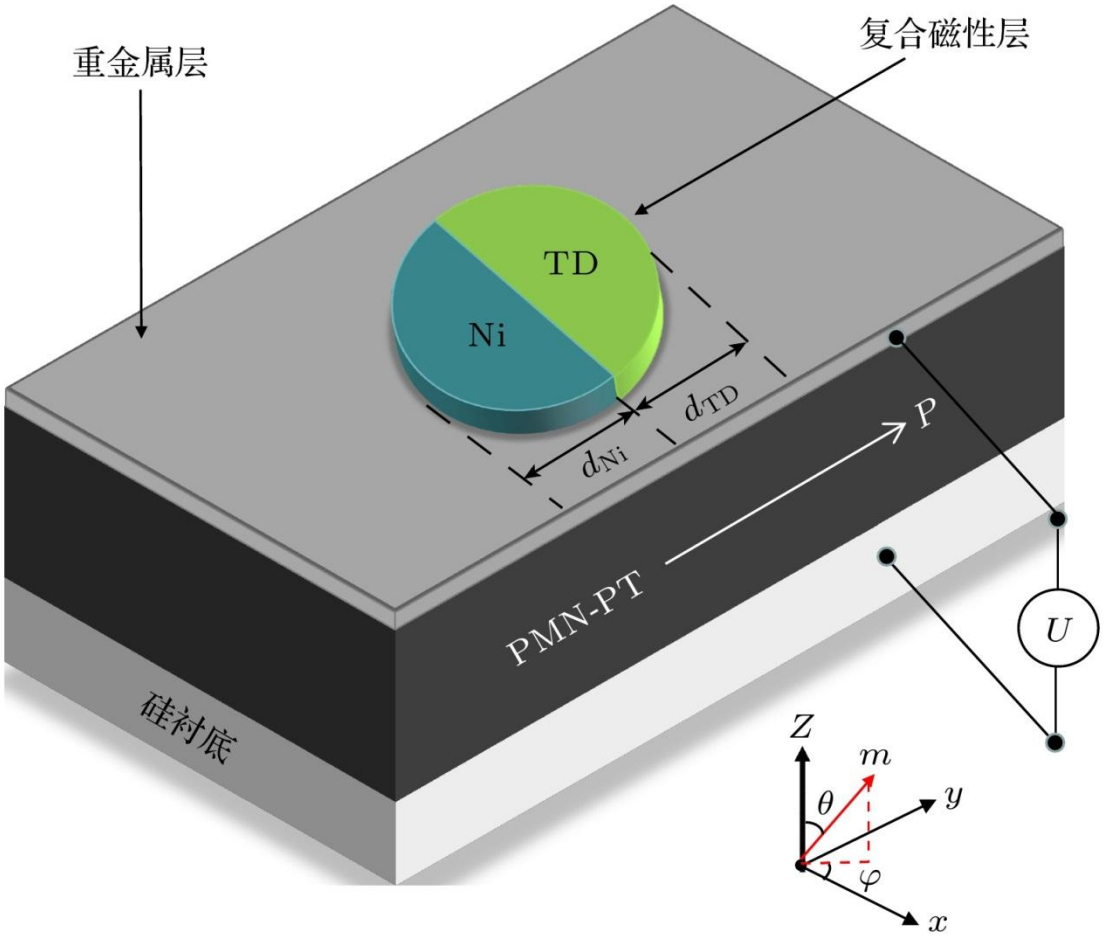

Figure 2. Diagram of bicomponent multiferroic nanomagnets

In this paper, the magnetization dynamics of a bicomponent nanomagnet is simulated by using the GPU-based micromagnetic simulation software MuMax$_3$. The MuMax$_3$ uses the finite element method to calculate the magnetization dynamics of a nanomagnet varying with time and space[23]. The Landau-Lifshitz-Gilbert (LLG) equation in the MuMax$_3$ is given by the following[24-26]:

$$\frac{\partial \boldsymbol{m}}{\partial t} = \gamma_{\mathrm{LL}} \frac{1}{1+\alpha^2}\{\boldsymbol{m} \times \boldsymbol{B}_{\mathrm{eff}} + \alpha[\boldsymbol{m} \times (\boldsymbol{m} \times \boldsymbol{B}_{\mathrm{eff}})]\}, \qquad (1)$$

Where $\boldsymbol{m}$ is the magnetization vector, γ_{LL} is the LLG gyromagnetic ratio, α is the LLG damping coefficient, and $\boldsymbol{B}_{\mathrm{eff}}$ is the effective field, i.e.

$$\boldsymbol{B}_{\mathrm{eff}} = \boldsymbol{B}_{\mathrm{exch}} + \boldsymbol{B}_{\mathrm{demag}} + \boldsymbol{B}_{\mathrm{DM}} + \boldsymbol{B}_{\mathrm{stress}}. \qquad (2)$$

Where the effective field $\boldsymbol{B}_{\mathrm{eff}}$ consists of the exchange field $\boldsymbol{B}_{\mathrm{exch}}$, the demagnetizing field $\boldsymbol{B}_{\mathrm{demag}}$, the DMI field $\boldsymbol{B}_{\mathrm{DM}}$ and the stress anisotropy field $\boldsymbol{B}_{\mathrm{stress}}$. There is no stress anisotropy field in MuMax$_3$ simulation software, because the uniaxial magnetocrystalline anisotropy of polycrystalline magnetostrictive materials is negligible, so this paper uses the

uniaxial magnetocrystalline anisotropy field to simulate the stress anisotropy field[27]. In MuMax$_3$, the uniaxial magnetocrystalline anisotropy field is expressed as

$$\boldsymbol{B}_{\text{anis}} = \frac{2K_{u1}}{B_{\text{sat}}}(\boldsymbol{u}\cdot\boldsymbol{m})\boldsymbol{u} + \frac{4K_{u2}}{B_{\text{sat}}}(\boldsymbol{u}\cdot\boldsymbol{m})^3\boldsymbol{u}, \qquad (3)$$

Where $\boldsymbol{u}$ is the unit vector of magnetocrystalline anisotropy, and K_{u1} and K_{u2} are the first-order and second-order uniaxial magnetocrystalline anisotropy constants. $B_{\text{sat}} = \mu_0 M_{\text{sat}}$. The uniaxial stress anisotropy field can be expressed as

$$\boldsymbol{B}_{\text{stress}} = \frac{3\lambda_s\sigma}{B_{\text{sat}}}(\boldsymbol{s}\cdot\boldsymbol{m})\boldsymbol{s}, \qquad (4)$$

Where λ_s is the magnetostriction coefficient, σ is the uniaxial stress (Pa), and $\boldsymbol{s}$ is the unit vector of stress, assuming a $K_{u2} = 0$, so that the K_{u1} can be regarded as

$$K_{u1} = \frac{3\lambda_s\sigma}{2}. \qquad (5)$$

Therefore, the contribution of the uniaxial stressσ to the effective field can be replaced by the uniaxial magnetocrystalline anisotropy field of MuMax$_3$. When a voltage is applied to an electrode whose size is equivalent to the thickness of the piezoelectric film, a local strain field will be generated under the electrode according to the inverse piezoelectric effect, and whether the strain is compressive or tensile depends on the polarity of the voltage[28,29]. Assuming that the strain is completely transferred from the piezoelectric layer to the nanomagnetic disk, the magnetostriction coefficients of Ni and Terfenol-D are opposite, so when the same polarity voltage is applied, the opposite strain will be generated in the region of different material components. Due to the inverse magnetostrictive effect, the opposite strain leads to opposite magnetization responses in different material regions[30].

3. Results and Discussion

3.1 Effect of Material Ratio, DMI, Size and Shape on MRV of Bicomponent Nanomagnet

In the absence of external excitation and with the same size, the bicomponent nanomagnets with different material ratios can obtain a variety of magnetic moment structures in the face of DMI with different strengths, including single-domain state, multi-domain state, toroidal magnetic vortex, radial magnetic structure, classical magnetic vortex and Skyrmion. Therefore, when designing nanodisks, the choice of material ratio plays a vital role in their magnetization state under DMI. These various magnetization states are actually the result of the complex and subtle

interaction and competition among the demagnetization energy, the exchange interaction energy and the DMI energy. The exchange energy originates from the exchange of the magnetic moments of the adjacent atoms, which tends to be parallel under the drive of the exchange interaction, and the exchange energy shows the energy characteristics of a short-range force. The demagnetization energy originates from the dipole-dipole interaction between the atomic magnetic moments in the ferromagnetic system, and its influence is more far-reaching, belonging to the category of long-range interaction energy. A characteristic size, the exchange length, is formed in the competition between the magnetostatic energy and the exchange interaction energy:

$$l_{\text{exch}} = \sqrt{\frac{A}{\mu_0 M_S^2}}. \qquad (6)$$

The exchange length of the two ferromagnetic materials used in this paper is greater than 2nm, so the minimum simulation unit is 2nm×2nm×1nm. DMI is an asymmetric exchange interaction due to spin-orbit coupling, which tends to force adjacent magnetic moments to align perpendicularly in heterostructures lacking interfacial inversion symmetry. Therefore, the presence of DMI can pull the in-plane magnetic moment in the magnetic vortex to the vertical direction, thus causing novel changes in the magnetic structure. The ground state of bicomponent nanomagnets with different material ratios is different, so the stability of MRV is related to the material ratio. Firstly, the micromagnetic simulation study is carried out for the two material ratios of the bicomponent nanomagnet, in order to find the most appropriate material ratio to form a stable MRV in the bicomponent nanomagnet disk. Based on the LLG equation, the spin dynamics model of the structure was established by using $MuMax_3$ simulation software. The RK45 solver was used, the fixed step size was set to 10^{-13}s, and the temperature was set to 0 K. In addition, due to the interfacial exchange interaction between materials, the exchange interaction constant at the interface needs to be set to the harmonic average of the exchange interaction constants of the two ferromagnetic materials. In the micromagnetic simulation, the thickness of the bicomponent nanomagnet nanodisk is 1 nm, the radius is 50 nm, the DMI coefficient *D* is set to a fixed value of 1.7 mJ/m^2, and the initial magnetization state is set to be a chiral vortex (P = 1, R = 1), and then five different material ratios are selected to find the energy minimum of the nanodisk magnetization state by the conjugate gradient method, and the simulation results are shown in Fig. 3. From the results, when the appropriate *D* value is selected, the bicomponent nanomagnet with different material ratios can achieve stable radial magnetic vortex, but the position of the vortex core will change with the material ratio, which is the result of the energy competition between the two material systems, so that the total energy of the bicomponent nanomagnet is always kept at the lowest value that the system can achieve, that is, the ground state. In order to improve the readout rate of the vortex and take into account the redundancy of manufacturing errors, the ratio of the two materials in the bicomponent nanomagnet is selected as $d_{\text{TD}} : d_{\text{Ni}} = 1 : 2$.

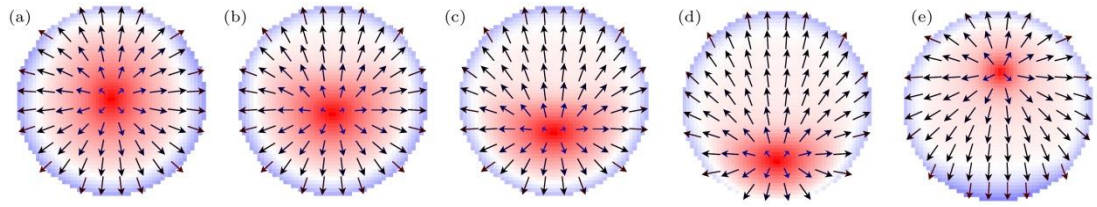

Figure 3. Ground states of bicomponent nanomagnets with different ratios

The control variable method was used to explore the influence of the DMI coefficient *D* on the MRV steady state of the bicomponent nanomagnet disk by changing the DMI coefficient *D*. The experimental results are shown in the Fig. 4. When the diameter and thickness of the bicomponent nanomagnet are fixed and the *D* value is lower than $1.2\ \mathrm{mJ/m^2}$, the exchange interaction energy plays a dominant role due to the weakening of the DMI effect, and the bicomponent nanomagnet presents a single-domain state. When the value of *D* is higher than $1.9\ \mathrm{mJ/m^2}$, the energy cannot maintain the equilibrium of the radial magnetic vortex state, resulting in the appearance of domain walls. The increase of the number of domain walls minimizes the DMI energy, the system reaches equilibrium again, and the interior of the bicomponent nanomagnet becomes a multi-domain state. Only when the *D* value is between $1.2\ \mathrm{mJ/m^2}$and $1.9\ \mathrm{mJ/m^2}$, the DMI effect is dominant, and the stable radial magnetic vortex state can be maintained in the bicomponent nanomagnet. In the above range of DMI coefficients, the effects of the diameter and thickness of the bicomponent nanomagnet on the radial magnetic vortex state are also studied. The results are shown in Fig. 5. When the thickness of the nanomagnet is less than 4 nm, the appropriate radius can be found to make the ground state of the bicomponent nanomagnet radial magnetic vortex state, especially when the thickness is $= 1\mathrm{nm}$, the radius of the bicomponent nanomagnet can maintain the radial magnetic vortex in the $(50 \pm 10)\mathrm{nm}$ range.

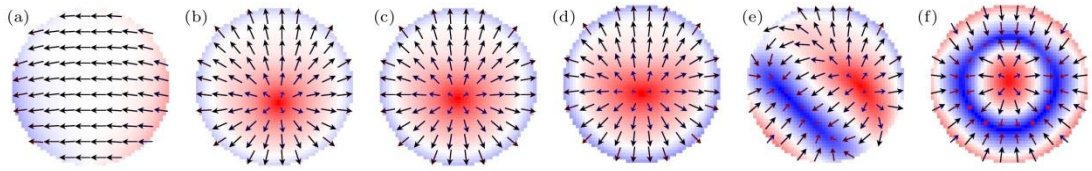

Figure 4. Ground states of the bicomponent nanomagnets with different DMI factors when the material ratio is $d_{\mathrm{TD}}{:}\,d_{\mathrm{Ni}} = 1{:}\,2$.

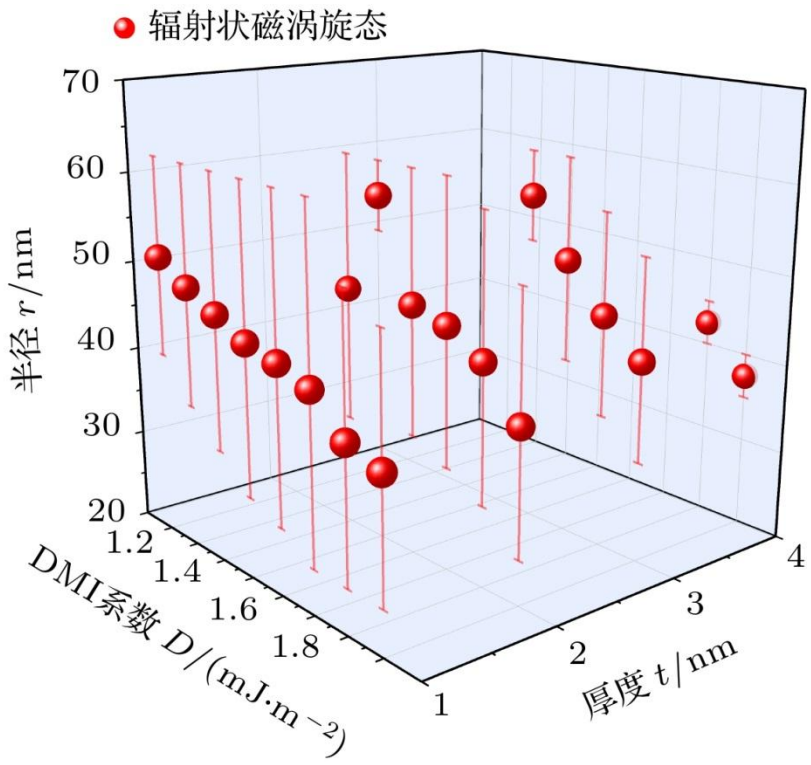

Figure 5. The influence of the diameter and thickness of bicomponent nanomagnets on the state of radial magnetic vortices

In addition, this paper also verifies whether the square and elliptical bicomponent nanomagnets have radial magnetic vortex ground States. The results are shown in Fig. 6. In the above DMI range, the square with a side length of 100nm and the elliptical bicomponent nanomagnets with a major axis of 120nm and a minor axis of 100nm both have stable radial magnetic vortex ground States. The above results prove that the bicomponent nanomagnet designed in this paper has good error redundancy, which lays a foundation for the subsequent experimental preparation.

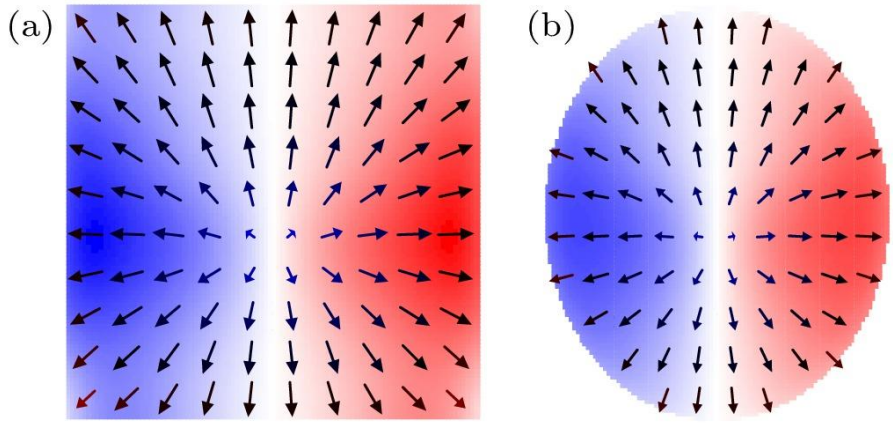

Figure 6. Radiating magnetic vortices of different shapes

3.2 Verification of MRV function of strain-regulated bicomponent nanomagnet

The effects of different material ratios and DMI coefficients on the ground state of bicomponent nanomagnets were discussed above. According to the above results, a bicomponent nanomagnet with a material ratio of $d_{\mathrm{TD}}: d_{\mathrm{Ni}} = 1:2,\ D = 1.7\mathrm{mJ/m^2}$ was selected in this section, and the control results of strain on the MRV polarity of bicomponent nanomagnets were verified by micromagnetic simulation. In this section, we introduce the parameter of the number of Skyrmions to distinguish different magnetic moment structures such as MRV, single domain, and Skyrmion. Specifically, these structures have different values of Skyrmions: the number of Skyrmions for the MRV is between 0.7 and 0.9, while that of the toroidal magnetic vortex is 0.5. Therefore, whether the MRV is reversed or not can be judged according to the change of the *S* of the Schluminger number with time:

$$S = \frac{1}{4\pi}\iint q \cdot \mathrm{d}x\mathrm{d}y, q = m \cdot (\frac{\partial m}{\partial x} \times \frac{\partial m}{\partial y}), \qquad (7)$$

Where q is the topological density[31].

To compare the difference between bicomponent nanomagnets and nanomagnets composed of a single material, all Ni and all Terfenol-D nanomagnets were selected as controls for simulation experiments. A voltage of 90 mV($\sigma = -120\mathrm{MPa}$) was applied to the three nanomagnets for 10 ns, and the polarity reversal of MRV in the bicomponent nanomagnet was observed. The simulation results are shown in the Fig. 7. The results show that the magnetization States of the three nanomagnets tend to be stable after 10 ns of stress application. Through the analysis of the magnetization state of the three kinds of nanomagnets at 10 ns, it can be concluded that the nanomagnet composed of Ni can be transformed into a single domain state under stress; The radial magnetic vortex state of all Terfenol-D nanomagnets is not destroyed due to the small applied stress; In the bicomponent nanomagnet, the original radial magnetic vortex core disappears under the action of strain, and a new radial magnetic vortex core with opposite polarity appears at the edge of the disk. Therefore, once the voltage is removed, the new core at the edge of the bicomponent nanomagnet moves toward its center, eventually reversing the MRV polarity. It can be seen that a single material cannot achieve strain-controlled MRV polarity reversal, while a bicomponent nanomagnet breaks through the limitation of a single material magnetic layer and can achieve field-free strain-controlled MRV polarity reversal by using the different responses of two materials with opposite magnetostrictive coefficients to opposite strains.

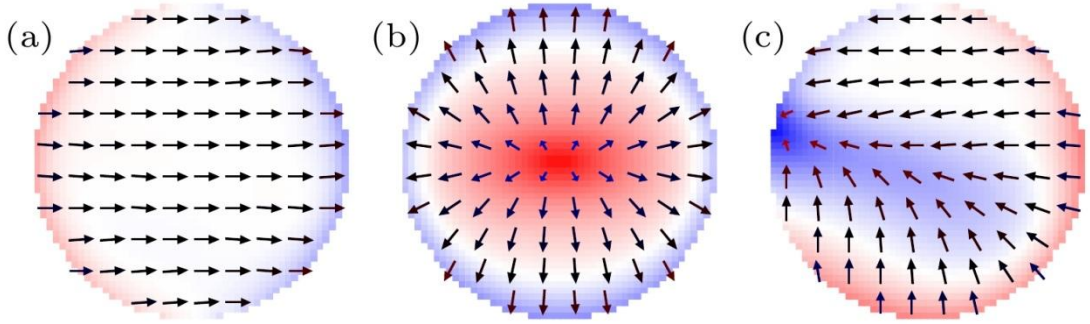

Figure 7. Magnetization states of three types of nanomagnets after 10 ns of stress action

In order to verify the above inference, further simulation studies are carried out. The Fig. 8 shows the variation of the number of Skyrmions and the normalized magnetization component m_z with time when two square-wave voltages with a period of *T*=15ns are applied to the bicomponent nanomagnet. In each voltage cycle, a positive voltage of 90 mV is first applied for 10ns, and then the voltage is removed, allowing the bicomponent nanomagnet to naturally relax for 5ns to reach a steady state. The simulation results show that in the first cycle, the normalized magnetization component m_z of the bicomponent nanomagnet in the *z* direction changes from 0.16 to –0.16, and the number of Skyrmions *S* changes from 0.7 to –0.7. After the second strain cycle, the m_z and *S* change to 0.16 and 0.7. The changes of these parameters indicate that the strain clock can effectively control the polarity reversal of MRV, and the control method is reversible.

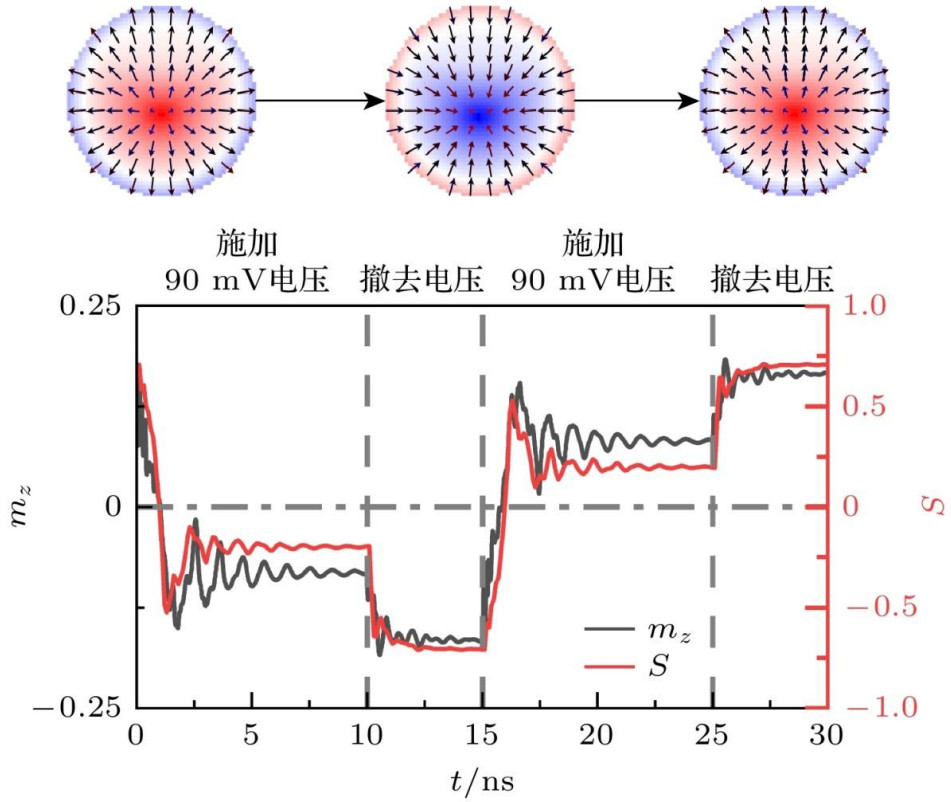

Figure 8. Variation with time of the normalized magnetization component m_z and the skyrmion number *S* of a bicomponent nanomagnet under the action of a strain clock

3.3 Internal mechanism of strain-regulated bicomponent nanomagnet MRV

In order to further explore the effect of strain on MRV switching of bicomponent nanomagnets, Fig. 9 shows the magnetization distribution and energy change curves at different time points during the application of cyclic strain. According to Fig. 9(b), Terfenol-D material has a positive magnetostriction coefficient and Ni has a negative magnetostriction coefficient, so the two materials produce opposite magnetization precession responses under the same strain in the first 10 ns of applied voltage. Specifically, under the action of voltage, the upper part of the magnetic moment of MRV tends to align along the *x-axis*, while the lower part of the magnetic moment tends to align along the *y-axis*. This opposite tendency of magnetization precession breaks the symmetry of MRV, causing the old radial magnetic vortex core to be driven to the edge of the disk and annihilated, and then a new anti-radial magnetic vortex core is formed at the edge, and the in-plane magnetization gradually points to the new radial magnetic vortex core. At the same time, it can be observed from the Fig. 9(a) that the demagnetization energy of MRV decreases and the exchange interaction energy increases, which indicates that the exchange interaction energy plays a dominant role in the polarity reversal process. When the time reaches t = 10 ns, the magnetization distribution of MRV reaches a steady state. Within 5 ns after the voltage is removed, due to the stress anisotropy returning to zero, the balance of the magnetization distribution is broken again, the anti-radial magnetic vortex core loses its binding and gradually returns to the center from the edge, the demagnetization energy of the MRV increases, while the exchange interaction energy decreases, and the MRV naturally relaxes to the steady state of the MRV, thus completing the polarity reversal of the MR. From the overall switching process, the total energy of MRV shows a downward trend, which reflects the characteristics of magnetization distribution, that is, the magnet tends to achieve the state of minimizing the total energy. In the process of polarity reversal, the change trend of demagnetization energy is opposite to that of exchange interaction energy, and the energy competition between the two material systems drives the reconstruction of the magnetic moment to achieve efficient and ultra-low energy consumption MRV polarity reversal.

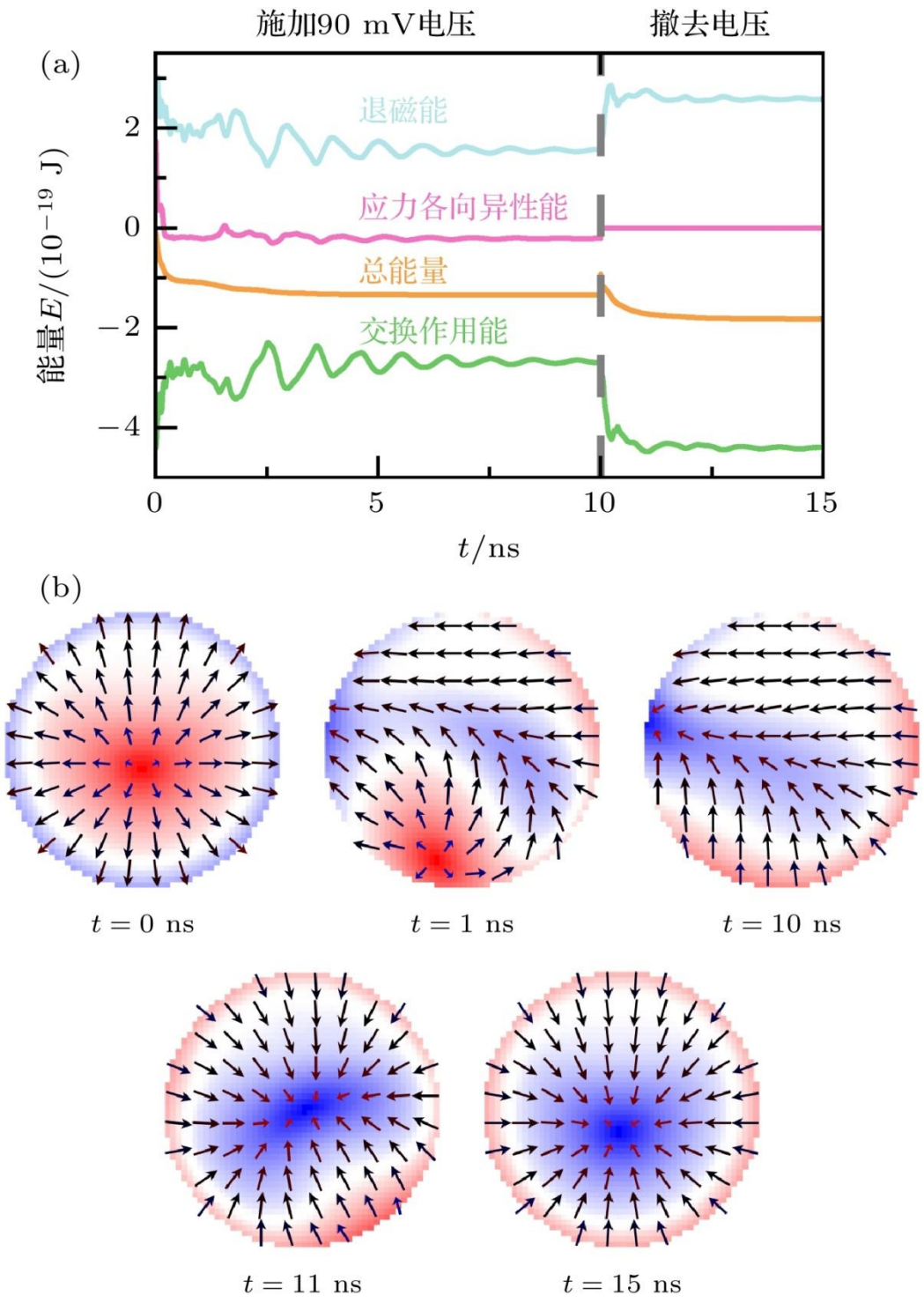

Figure 9. Energy variation and transient diagram of the polarity inversion process of MRV under the action of the strain clock

3.4 Strain-regulated energy consumption per turnover of bicomponent nanomagnet MRV

According to the calculation method of energy consumption per bit switching provided by reference [32], the energy consumption E_{total} of the strain control technology proposed in this paper during MRV switching mainly comes from the energy consumption E_{internal} caused by

the Gilbert damping inside the bicomponent nanomagnet and the strain clock energy consumption E_{strain}. Where the expression for E_{internal} is

$$E_{\mathrm{internal}} = \int_0^{\tau} \frac{\alpha \mu_0 \gamma V}{(1+\alpha^2) M_{\mathrm{s}}} |\boldsymbol{H}_{\mathrm{eff}} \times \boldsymbol{M}|^2 \mathrm{d}t, \qquad (8)$$

Whereτ is the precession time of the magnetic moment vector of the bicomponent nanomagnet. The calculated E_{internal} of the bicomponent nanomagnet is 2 aJ.

The E_{strain} is mainly caused by the parasitic capacitance of the piezoelectric layer. The electrode plate and the substrate can be regarded as two parallel plate capacitors, so the piezoelectric layer is the insulating medium inserted between them. The relative permittivity of PMN-PT is $\varepsilon_{\mathrm{r}} = 1000$, so the parasitic capacitance of the piezoelectric layer is $C_{\text{PMN-PT}}$.

$$C_{\mathrm{PMN-PT}} = \frac{\varepsilon_0 \varepsilon_{\mathrm{r}} S}{h_{\mathrm{PMN-PT}}}, \qquad (9)$$

Where $\varepsilon_0 = 8.85 \times 10^{-12} \mathrm{F/m}$ is the vacuum dielectric constant, and S is the facing area of the electrode plate.When a strain of 90 mV is applied to the MRV, the strain clock energy E_{strain} consumed by the MRV is

$$E_{\mathrm{strain}} = C_{\mathrm{PMN-PT}} U^2. \qquad (10)$$

Calculated $E_{\mathrm{strain}} \approx 3.6$ aJ. Therefore, for strain-regulated bicomponent MRV polarity reversal, the total energy E_{total} consumption per bit reversal is 5.6 aJ. For bicomponent nanomagnet MRV with other material proportions and sizes, the specific energy consumption varies slightly with the amplitude and pulse width of the voltage signal, and the total energy consumption can be less than 10 aJ/bit. The energy consumption of the traditional STT control method is about 1 pJ/bit[14] due to the Joule heating caused by the current. In contrast, the energy consumption of the strain control method used in this paper is reduced by 6 orders of magnitude, and the power consumption is very low.

4. Conclusion

In this paper, a multiferroic heterostructure composed of a bicomponent nanomagnet (Terfenol-D/Ni), a heavy metal layer, and a piezoelectric layer is proposed, and its unique strain-regulated magnetic vortex (MRV) polarity reversal mechanism is revealed through theoretical modeling and simulation verification. The system can stably maintain the radial magnetic vortex state in the range of bicomponent nanomagnet material ratio $d_{\mathrm{TD}} : d_{\mathrm{Ni}} = 1:2$

and Dzyaloshinskii-Moriya interaction coefficient ($1.2\mathrm{mJ/m^2} < D < 1.9\mathrm{mJ/m^2}$), and when the DMI coefficient is equal to $1.7\ \mathrm{mJ/m^2}$, the MRV polarity reversal can be achieved with only 90 mV voltage pulse, and the energy consumption is reduced by 6 orders of magnitude to aJ level compared with the traditional spin current regulation. Through transient dynamics and energy analysis, the microscopic mechanism of strain-driven polarity reversal is clarified, and the significant advantages of the scheme in low power consumption and high speed response are verified. This study not only provides a feasible technical path for the on-chip integration of magnetic vortex memory devices, but also expands the control dimension of non-current-driven "electro-writing" magnetic memory devices by introducing the design of bicomponent multiferroic nanomagnets, which provides an important theoretical basis and experimental reference for the future development of low-power and high-density magnetic memory technology.

References

[1] Yamada K, Kasai S, Nakatani Y, Kobayashi K, Kohno H, Thiaville A, Ono T 2007 *Nat. Mater.* **6** 270

[2] Dong D N, Cai L, Li C, Liu B J, Li C, Liu J H 2018 *Acta Phys. Sin.* **67** 228502

[3] Siracusano G, Tomasello R, Giordano A, Puliafito V, Azzerboni B, Ozatay O, Carpentieri M, Finocchio G 2016 *Phys. Rev. Lett.* **117** 087204

[4] Hrabec A, Porter N, Wells A, Benitez M, Burnell G, McVitie S, McGrouther D, Moore T, Marrows C 2014 *Phys. Rev. B: Condens. Matter* **90** 020402

[5] Tomasello R, Carpentieri M, Finocchio G 2014 *J. Appl. Phys.* **115** 17C730

[6] Verba R, Navas D, Hierro-Rodriguez A, Bunyaev S, Ivanov B, Guslienko K, Kakazei G 2018 *Phys. Rev. Appl.* **10** 031002

[7] Bhattacharjee P, Mondal S, Saha S, Barman S 2025 *J. Phys. Condens. Matter* **37** 133001

[8] Karakas V, Gokce A, Habiboglu A T, Arpaci S, Ozbozduman K, Cinar I, Yanik C, Tomasello R, Tacchi S, Siracusano G 2018 *Sci. Rep.* **8** 7180

[9] Li C, Cai L, Wang S, Yang X, Cui H, Wei B, Dong D, Li C, Liu J, Liu B 2018 *IEEE Trans. Magn.* **54** 3400806

[10] Wang Y, Wang L, Xia J, et al. 2020 *Nat. Commun.* **11** 3577

[11] Schoenherr P, Manz S, Kuerten L, Shapovalov K, Iyama A, Kimura T, Fiebig M, Meier D 2020 *npj Quantum Materials* **5** 86

[12] Geirhos K, Gross B, Szigeti B G, Mehlin A, Philipp S, White J S, Cubitt R, Widmann S, Ghara S, Lunkenheimer P, et al. 2020 *npj Quantum Materials* **5** 44

[13] Li C, Fang L, Yang X, Xu N, Liu B, Wei B, Zhou E, Yang B 2019 *J. Phys. D: Appl. Phys.* **53** 015001

[14] Ma Y, Zhao R, Song C, Jin C, Wang J, Wei Y, Huang Y, Wang J, Wang J, Liu Q

2019 *J. Magn. Magn. Mater.* **491** 165544
[15] Dong D, Cai L, Li C, Liu B, Li C, Liu J 2019 *J. Phys. D: Appl. Phys.* **52** 295001
[16] Fujita R, Gurung G, Mawass M A, et al. 2024 *Adv. Funct. Mater.* **34** 2400552
[17] Zhu M, Hu H, Cui S, Li Y, Zhou X, Qiu Y, Guo R, Wu G, Yu G, Zhou H 2021 *Appl. Phys. Lett.* **118** 262412
[18] Hu H, Yu G, Li Y, Qiu Y, Zhu H, Zhu M, Zhou H 2022 *Micromachines* **13** 1056
[19] Sanchez-Manzano D, Orfila G, Sander A, et al. 2024 *ACS Appl. Mater. Interfaces* **16** 19681
[20] Shimon G, Adeyeye A, Ross C 2012 *Appl. Phys. Lett.* **101** 083112
[21] Xia Y, Yang X, Dou S, Cui H, Wei B, Liang B, Yan X 2024 *AIP Adv.* **14** 045239
[22] Biswas A K, Bandyopadhyay S, Atulasimha J 2014 *Appl. Phys. Lett.* **105** 072408
[23] Vansteenkiste A, Leliaert J, Dvornik M, Helsen M, Garcia-Sanchez F, Van Waeyenberge B 2014 *AIP Adv.* **4** 107133
[24] Landau L, Lifshitz E 1935 *Phys. Z. Sowjetunion* **8** 101
[25] Gilbert T L 1955 *Phys. Rev.* **100** 1243
[26] Zhang S, Wang W, Burn D, Peng H, Berger H, Bauer A, Pfleiderer C, Van Der Laan G, Hesjedal T 2018 *Nat. Commun.* **9** 2115
[27] Cui H, Cai L, Yang X, Wang S, Zhang M, Li C, Feng C 2018 *Appl. Phys. Lett.* **11** 092404
[28] Cui J, Hockel J L, Nordeen P K, Pisani D M, Liang C y, Carman G P, Lynch C S 2013 *Appl. Phys. Lett.* **103** 232905
[29] Cui J, Liang C Y, Paisley E A, Sepulveda A, Ihlefeld J F, Carman G P, Lynch C S 2015 *Appl. Phys. Lett.* **107** 092903
[30] Bandyopadhyay S 2024 *IEEE Trans. Magn.* **60** 1
[31] Nagaosa N, Tokura Y 2013 *Nat. Nanotechnol.* **8** 899
[32] Dou S, Yang X, Yuan J, Xia Y, Bai X, Cui H, Wei B 2023 *IEEE Magn. Lett.* **14** 4500305